

Neutrino Trident Production at the Intensity Frontier

Gabriel Magill^{1,2,*} and Ryan Plestid^{1,2,†}

¹*Department of Physics & Astronomy, McMaster University, 1280 Main St. W., Hamilton, Ontario, Canada*

²*Perimeter Institute for Theoretical Physics, 31 Caroline St. N., Waterloo, Ontario, Canada*

(Dated: December 20, 2016)

We have calculated cross sections for the production of lepton pairs by a neutrino incident on a nucleus using both the equivalent photon approximation, and deep inelastic formalism. We find that production of mixed flavour lepton pairs can have production cross sections as high as 35 times those of the traditional $\nu_\mu \rightarrow \nu_\mu \mu^+ \mu^-$ process. Rates are estimated for the SHiP and DUNE intensity frontier experiments. We find that multiple trident production modes, some of which have never been observed, represent observable signals over the lifetime of the detectors. Our estimates indicate that the SHiP collaboration should be able to observe on the order of 300 trident events given $2 \cdot 10^{20}$ POT, and that the DUNE collaboration can expect approximately 250 trident events in their near detector given $3 \cdot 10^{22}$ POT. We also discuss possible applications of the neutrino trident data to be collected at SHiP and DUNE for SM and BSM physics.

PACS numbers: 12.15.Ji, 13.15.+g, 13.60.Hb, 14.60.-z

I. INTRODUCTION

Neutrino physics has traditionally been dominated by the measurement of oscillation parameters and the study of neutrino nucleus scattering. These experimental signals are largely dominated by charged current (CC), and neutral current (NC) interactions whose cross sections scale as $\sigma \sim s G_F^2$. Traditionally, limits on beam luminosity have resulted in event counts that leave subdominant processes with expected event rates less than unity in the lifetime of an experiment. As a result these processes are often omitted in the discussions of neutrino physics. One such neglected process is neutrino trident production which has been previously observed at CHARM II, CCFR, and NuTeV [11, 15, 16]. These measurements provided evidence at the 3σ level for the contribution of Z bosons in weak interactions [15], and more recently have been used to constrain BSM physics. Specifically, measurements from CCFR currently provide the best constraints on the mass and coupling of a heavy Z' force-mediator charged under $L_\mu - L_\tau$ [2]. Both of these applications are successful because the neutrino trident production of leptons is sensitive to both the vector and axial current couplings (see Section II A).

The aforementioned collaborations only measured one possible mode of trident production; specifically $\nu A \rightarrow \nu \mu^+ \mu^- A$. The leading order contribution to this process involves the production of a muon-anti-muon pair, which can then interact with the target nucleus A electromagnetically (see Fig. 1). For low momentum transfers ($Q \ll R_A^{-1}$) the nucleus interacts coherently with the virtual photons ($\sigma \propto Z^2$), and there is a strong enhancement due to the infrared divergence in the photon propagator; it is this kinematic regime which dominates the

cross section. Other qualitatively similar processes, such as e^+e^- or μ^+e^- trident production, were kinematically accessible, however, due to technological limitations in the detector design, the required vertex resolution for trident identification was not achievable for electrons. This would not be an issue with modern detectors.

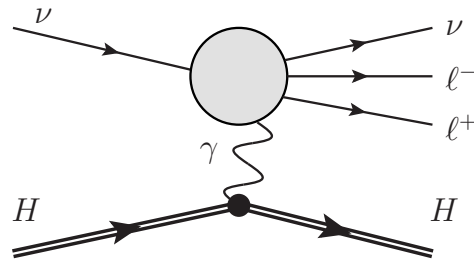


FIG. 1: Leading hadronic contribution to trident production. Arrows denote direction of momentum.

The cross section for $\mu^+ \mu^-$ neutrino trident production is approximately five orders of magnitude smaller than the charged current cross section ($\sigma \approx 10^{-5} \sigma_{CC}$) for a 50 GeV neutrino scattering off an iron nucleus [4]; high Z materials will have an even larger cross section relative to CC scattering. This means that practically trident production can only be observed in experiments with very large neutrino fluxes. Additionally the leading contribution to the cross section discussed in the preceding paragraph can be calculated using the equivalent photon approximation and scales as $\sigma \sim G_F^2 E_\nu Q_{\max} \log(E_\nu Q_{\max}/m_\ell^2)$, where m_ℓ is related to the lepton masses, and Q_{\max} is a characteristic momentum transfer set by the radius of the nucleus [4]. These considerations imply that for trident to be a useful tool one needs to consider experiments with both a high energy neutrino beam ($\langle E_\nu \rangle \gtrsim 1$ GeV), and high statistics. This can be achieved via beam luminosity, or

* gmagill@perimeterinstitute.ca

† plestird@mcmaster.ca

target-mass considerations. Fixed target and beam dump experiments—where neutrino energies can be in excess of 100 GeV, and charged current event counts can exceed 10^6 —are an ideal setting to study neutrino trident production. The Search for Hidden Particles (SHiP) experiment and the Deep Underground Neutrino Experiment (DUNE) both fall into these categories, and, as we show in this paper, represent the newest frontier in the study of trident production.

SHiP’s program of study, as it relates to neutrino physics, is largely focused on tau neutrino, and anti-tau neutrino events, and is therefore optimized to observe tau leptons [19]. This represents a qualitatively new opportunity in the study of trident production, because the high mass of the tau leptons results in a threshold effect, wherein coherent production of a single tau lepton is not possible unless the following inequality holds $E_\nu > (1/2)m_\tau^2 R_A$; the bound for tau lepton pair production is given by $E_\nu > 2m_\tau^2 R_A$. As a result we also investigate the incoherent contribution to the cross section using both a diffractive and deep-inelastic approach. The experiment will use beams with $\langle E_\nu \rangle \approx 30 \text{ GeV} - 60 \text{ GeV}$, and expects a lifetime collection of charged current events on the order of $N_{\text{CC}} \approx 2.7 \cdot 10^6$ [19]. It is therefore reasonable to assume that mixed flavour trident production, possibly including tau leptons, should be observable at the SHiP experiment.

Although the focus of its program of study is neutrino oscillations, the Deep Underground Neutrino Experiment (DUNE) will use sufficiently high luminosities, and neutrino energies to induce trident production. DUNE consists of a near detector on site at FERMILAB [1] and a far detector at Sanford Lab, both composed of liquid argon. This technology allows for the observation of both electrons, and muons. The far detector is exposed to a flux of neutrinos after a 1300 km transit through earth. The near detector will be used to account for systematic uncertainties in the neutrino beam and to record the initial neutrino flux. It is designed to obtain ten times the statistics of the far detector [1]. The expected charged current event count in the far detector over the lifetime of the experiment is on the order of $1 \cdot 10^5$, and so it is reasonable to expect an observable signal of trident events for some of the processes; especially given the enhanced statistics of the planned near detector.

Trident production has proven itself a useful tool for constraining BSM physics by virtue of its sensitivity to modifications of C_A and C_V . Additionally it represents an experimental signal that would provide an obvious background to searches of lepton flavour violation in the case of multi-flavour charged-lepton tridents. If these new experiments (SHiP and DUNE) are to use trident production to probe BSM physics, then it is imperative to understand the relevant Standard Model backgrounds.

The rest of this article is organized as follows: In Section II A we discuss the basic structure of the trident amplitude in the Standard Model. In Section II B we describe how to obtain the cross sections for three distinct

kinematic regimes; each receiving a separate theoretical treatment. In Section III we calculate expected rates, and cross sections for both DUNE and SHiP. We also present differential distributions with respect to the invariant mass of the charged lepton pair. In Section IV we review the qualitative features of our results and outline possible applications of trident for both SHiP and DUNE. Finally in Section V we discuss future directions for trident production for the upcoming generation of accelerator based neutrino experiments.

II. TRIDENT PRODUCTION IN THE STANDARD MODEL

A. Leptonic Matrix Element

Our treatment of trident production varies over kinematic regimes, characterized by the four-momentum transfer to the nucleus Q^2 . In every approach we treat the leptonic matrix element involving the EM current consistently. Our treatment of the nucleus’ interaction with the EM field, however, varies, and so will be treated separately in each section. In the lower Q^2 regimes we relate the cross section to that of a neutrino-photon collision (photo-trident production), while for large Q^2 we employ the parton model. The amplitudes for photo-trident production and parton-trident production can be written

$$\begin{aligned} i\mathcal{M}_{\gamma\nu} &= \epsilon^\mu L_\mu & (\text{EPA}) \\ i\mathcal{M}_{h\nu} &= \frac{-\eta^{\mu\nu}}{q^2} h_\nu L_\mu & (\text{DIS}) \end{aligned} \quad (1)$$

where ϵ^μ is an on-shell polarization tensor, and h_ν is the hadronic matrix element in the parton model. The leptonic matrix element L_μ is calculated explicitly below. We study both neutrino, and anti-neutrino induced trident production, and for the remainder of this section all reactions will contain an implicit hadronic initial and final state. We use Latin flavour indices $i, j, k \in \{e, \mu, \tau\}$ and consider reactions of the form

$$\{\nu_i \rightarrow \nu_i \text{ or } k + \ell_j^- + \ell_k^+, \quad \bar{\nu}_i \rightarrow \bar{\nu}_i \text{ or } j + \ell_j^- + \ell_k^+\}$$

with the constraint that generational lepton number is conserved. Both mono-flavour, and multi-flavour charged lepton pairs (i.e. $\mu^+\mu^-$ and $\mu^+\tau^-$) are included in our analysis. Assigning the labels $\{1, 2, 3, 4, 5\} \rightarrow \{\nu, \gamma, \nu', \ell^+, \ell^-\}$ with ν' the outgoing neutrino (see Fig. 2) and generalizing the analysis of [2, 21] to multi-flavour lepton pairs we find

$$\begin{aligned} L_{ijk}^\mu &= -\frac{ieG_F}{\sqrt{2}} \{ \bar{u}_3 \gamma^\alpha (1 - \gamma^5) u_1 \quad , \quad \bar{v}_1 \gamma^\alpha (1 - \gamma^5) v_3 \} \times \\ &\quad \bar{u}_5 \left[\gamma_\alpha (V_{ijk} - A_{ijk} \gamma^5) \frac{1}{\not{q} - \not{p}_4 - m_4} \gamma^\mu \right. \\ &\quad \left. + \gamma^\mu \frac{1}{\not{p}_5 - \not{q} - m_5} \gamma_\alpha (V_{ijk} - A_{ijk} \gamma^5) \right] v(p_4), \end{aligned} \quad (2)$$

ν Process	$\bar{\nu}$ Process	V_{ijk}	A_{ijk}	Mediator
$\nu_e \rightarrow \nu_e e^+ e^-$	$\bar{\nu}_e \rightarrow \bar{\nu}_e e^+ e^-$	$\frac{1}{2} + 2 \sin^2 \theta_w$	$\frac{1}{2}$	W,Z
$\nu_\mu \rightarrow \nu_\mu \mu^+ \mu^-$	$\bar{\nu}_\mu \rightarrow \bar{\nu}_\mu \mu^+ \mu^-$	$\frac{1}{2} + 2 \sin^2 \theta_w$	$\frac{1}{2}$	W,Z
$\nu_e \rightarrow \nu_\mu \mu^+ e^-$	$\bar{\nu}_e \rightarrow \bar{\nu}_\mu e^+ \mu^-$	1	1	W
$\nu_\mu \rightarrow \nu_e e^+ \mu^-$	$\bar{\nu}_\mu \rightarrow \bar{\nu}_e \mu^+ e^-$	1	1	W
$\nu_e \rightarrow \nu_e \mu^+ \mu^-$	$\bar{\nu}_e \rightarrow \bar{\nu}_e \mu^+ \mu^-$	$-\frac{1}{2} + 2 \sin^2 \theta_w$	$-\frac{1}{2}$	Z
$\nu_\mu \rightarrow \nu_\mu e^+ e^-$	$\bar{\nu}_\mu \rightarrow \bar{\nu}_\mu e^+ e^-$	$-\frac{1}{2} + 2 \sin^2 \theta_w$	$-\frac{1}{2}$	Z
$\nu_\mu \rightarrow \nu_\mu \tau^+ \tau^-$	$\bar{\nu}_\mu \rightarrow \bar{\nu}_\mu \tau^+ \tau^-$	$-\frac{1}{2} + 2 \sin^2 \theta_w$	$-\frac{1}{2}$	Z
$\nu_\mu \rightarrow \nu_\tau \mu^- \tau^+$	$\bar{\nu}_\mu \rightarrow \bar{\nu}_\tau \mu^+ \tau^-$	1	1	W
$\nu_\tau \rightarrow \nu_\mu \tau^- \mu^+$	$\bar{\nu}_\tau \rightarrow \bar{\nu}_\mu \tau^+ \mu^-$	1	1	W
$\nu_\tau \rightarrow \nu_\tau \mu^+ \mu^-$	$\bar{\nu}_\tau \rightarrow \bar{\nu}_\tau \mu^+ \mu^-$	$-\frac{1}{2} + 2 \sin^2 \theta_w$	$-\frac{1}{2}$	Z
$\nu_\tau \rightarrow \nu_\tau e^+ e^-$	$\bar{\nu}_\tau \rightarrow \bar{\nu}_\tau e^+ e^-$	$-\frac{1}{2} + 2 \sin^2 \theta_w$	$-\frac{1}{2}$	Z

TABLE I: Modified vector and axial coupling constants for different combinations of incident neutrino flavours and final states

where the first line contains the appropriate spinor wave-functions for an incident neutrino and anti-neutrino beam respectively. V_{ijk} and A_{ijk} are the flavour dependent vector and axial coupling strengths, which are typically denoted C_V and C_A respectively. We use non-standard notation to stress that these couplings carry flavour indices because some processes are mediated exclusively by W bosons, others exclusively by Z bosons, and some a mixture of the two. As we see from Fig. 2, these mediators modify the coupling to the vector and axial currents, as can be verified by use of Fierz identities. As noted in [4] the interference between the neutral and charged current channels in the Standard Model results in a 40% reduction in the cross section compared to the $V - A$ theory prediction. Thus by considering different combinations of leptons in the final state the cross section can be enhanced, or suppressed, significantly. The constants A_{ijk} and V_{ijk} are presented in Table I for $\nu_\mu \rightarrow \nu_\mu \tau^+ \tau^-$ and for all trident processes with lifetime event counts greater than 0.01 at either SHiP or DUNE.

B. Coherent, Diffractive and Deep Inelastic Regimes

We will begin by reviewing conventional scattering of neutrinos off of nuclei to emphasize the qualitative differences in trident production. Neutrino-nucleus scattering is dominated by charged current events, which can be loosely partitioned into three classes for $E_\nu \gtrsim 100$ MeV: quasi-elastic scattering, hadronic resonance production, and deep inelastic scattering [9]. It is only at low centre of mass energies $E \lesssim 50$ MeV that coherent scattering via the neutral current is possible such that the reaction's cross section scales as $\sigma \sim (A - Z)^2 E_\nu^2$ with $A - Z$ the number of neutrons. In this energy regime coherent scat-

tering cross sections can be as much as three orders of magnitude larger than that predicted by a naïve sum of the nucleon cross sections [8].

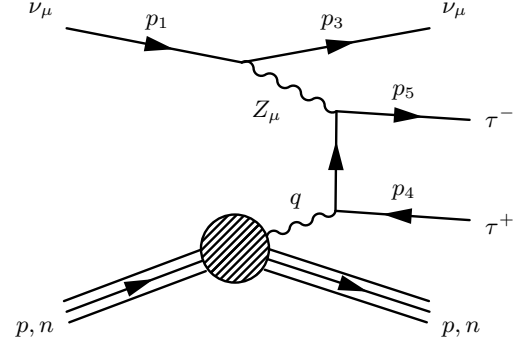


FIG. 2: An example of a process which takes place exclusively through the neutral current channel. The mismatch in flavour between the incident neutrino and outgoing leptons prohibits a charged current interaction.

This limited kinematic window stands in sharp contrast to trident production where coherent contributions are possible at all energies, because the reaction is not $2 \rightarrow 2$ and the phase space is therefore less kinematically constrained. This scattering is mediated electromagnetically, and, in addition to the coherent Z^2 amplification, the photon's propagator introduces an infrared divergence that further enhances the amplitude. As is the case for coherent neutrino scattering this regime is characterized by small momentum transfers ($Q^2 \sim R_A^{-2}$) wherein the phases of the various amplitudes are nearly commensurate, and the amplitudes interfere constructively. Kinematic considerations constrain the momentum transfer via $Q > s/(2E_\nu)$, with s the invariant mass of the neutrino-photon pair [4]. When combined with the lepton pair's mass threshold, this regulates the infrared divergence mentioned above. The three regimes typically considered in charged-current scattering for high energy neutrinos (mentioned in the first paragraph) also exist for trident production. Quasi-elastic-like diffractive scattering can contribute significantly to trident production, especially when threshold effects related to lepton masses are important. We expect the deep inelastic contribution to be suppressed, but for many of the neutrino energies at SHiP it is the only kinematically allowed production mechanism for tau leptons, and so we also include this regime in our analysis.

1. Coherent Regime

The coherent contribution to neutrino trident production can be accurately calculated using the equivalent photon approximation (EPA) [2, 4, 13, 20]. In the EPA the cross section for the full scattering process is decomposed into two pieces. First the cross section correspond-

ing to the scattering of a neutrino and photon creating a lepton trident, denoted by $\sigma_{\gamma\nu}$, is calculated. Next, this cross section is weighted against a universal probability distribution $P(s, Q^2)$ [2] that measures the likelihood of the nucleus producing a virtual photon with virtual-mass Q^2 , and neutrino-photon centre of mass energy s . The full cross section is given by

$$\begin{aligned}\sigma_{\nu A} &= \int ds \sigma_{\gamma\nu}(s) \int dQ^2 P(s, Q^2) \\ &= \frac{Z^2 \alpha}{\pi} \int_{m_{jk}^2}^{s_{\max}} \frac{ds}{s} \sigma_{\gamma\nu}(s) \int_{(s/2E_\nu)^2}^{\infty} \frac{dQ^2}{Q^2} F^2(Q^2)\end{aligned}\quad (3)$$

with $m_{jk} = m_j + m_k$ the sum of the lepton pair's masses. A fairly good, albeit crude, approximation is to treat the form-factor for the nucleus $F(Q^2)$ as a Heaviside function $\Theta(Q_{\max}^2 - Q^2)$ where the scale $Q_{\max} = \Lambda_{\text{QCD}}/A^{1/3}$ corresponds to characteristic momentum transfer at which one would expect the dissolution of the nucleus [4]. This sets a maximum centre-of-mass energy for the photon-neutrino interaction $s_{\max} = 2E_\nu Q_{\max}$. With these approximations, suppressing flavour indices and working in the leading log approximation, Eq. (3) simplifies to [2, 4]

$$\sigma_{\nu A} \approx \frac{1}{2}(A^2 + V^2) \frac{2 Z^2 \alpha^2 G_F^2}{9\pi^3} s_{\max} \log\left(\frac{s_{\max}}{4m^2}\right) \quad (4)$$

where $2m = m_j + m_k$. There are additional terms resulting from the interference between the vector and axial currents, but these are suppressed by two powers of the lepton mass, and are therefore small. A more realistic implementation is to use the Woods-Saxon form-factor, which is what we used in all of our calculations (this changes the answer by order 10%, see Appendix A for details). We can write the coherent contribution to the neutrino-nucleus cross section as

$$d\sigma_{\gamma\nu} = \frac{1}{2s} \frac{1}{2} \sum_{\text{pol}} |\epsilon_\mu L^\mu|^2 d\Phi_3 \quad (5)$$

where Φ_3 is the three-body phase space of final states, the factor of $1/2$ averages over photon polarizations, and $2s$ is the Lorentz invariant flux factor. For details on the treatment of the three-body phase space see Appendix A.

2. Diffractive Regime

At intermediate Q^2 it is possible to interact with the individual protons of the nucleus, both without coherent interference of their individual amplitudes, and without probing their inner parton structure. Our treatment of this regime follows the approach outlined in [6], and is identical to the coherent regime with the following changes:

$$\begin{aligned}\sigma_{\nu A} &= Z \int ds \sigma_{\gamma\nu}(s) \int dQ^2 P(s, Q^2) \\ &= Z \frac{\alpha}{\pi} \int_{m_{jk}^2}^{s_{\max}} \frac{ds}{s} \sigma_{\gamma\nu}(s) \int_{Q_{\min}^2}^{1 \text{ GeV}^2} \frac{dQ^2}{Q^2} F_{\text{dip}}^2(Q^2).\end{aligned}\quad (6)$$

The charge of the nucleus now appears as an overall multiplicative factor as opposed to appearing in $P(s, Q^2)$, we cut off our integral at $Q_{\min} = \max(s/2E_\nu, R_A^{-1})$ to avoid double counting amplitudes included in the coherent calculation, and we use the standard dipole fit to the proton's electromagnetic form factor (see Appendix A). We introduce an explicit UV cut-off for the Q^2 integration to avoid double counting with the DIS amplitudes. This was not necessary for the coherent regime due to the exponential, as opposed to power law, decay of the Wood-Saxon form factor at high Q^2 .

3. Deep Inelastic Regime

Our treatment of the deep inelastic case is fairly standard, with a few exceptions that are highlighted in Appendix B2. We treat this regime by convoluting the parton cross sections with nucleon parton distribution functions (PDFs) $f(\xi, Q)$ [14], taking into account the u, d, c, s quarks. The phase space integrals are sensitive to the lepton masses, and so although their effects on the matrix element are often sub-leading, we include their full dependence throughout our calculations. All of the quarks are treated as massless in our analysis.

We take care to include a cut on momentum transfers so as not to double count contributions already accounted for by the EPA. Additionally we place a cut on the momentum fraction ξ to ensure the parton carries enough four-momentum to both be able to produce the appropriate pair of charged leptons and to satisfy the double-counting-cut on momentum transfer. The resulting cross sections for the various nucleons are then summed to obtain the scattering cross section with the nucleus. We can write $\sigma_{\nu A}$ as a weighted sum of the cross sections with the constituent nucleons

$$\sigma_{\nu A} = Z\sigma_{\nu p} + (A - Z)\sigma_{\nu n}. \quad (7)$$

These can in turn be written in terms of the parton-level cross sections $\sigma_{h\nu}$ via

$$\sigma_{\nu H} = \sum_h \int_{\xi_{\min}}^1 d\xi \int_{Q_{\min}}^{Q_{\max}} dQ \frac{d\sigma_{h\nu}}{dQ}(\xi, Q) f_h^{(H)}(\xi, Q) \quad (8)$$

where $f_h^{(H)}(\xi, Q)$ is the PDF for parton h in the nucleon $H \in \{n, p\}$. More details can be found in Appendix B.

III. PROSPECTS AT FUTURE EXPERIMENTS

In the following, we calculate trident rates at SHiP, and at the DUNE far and near detectors. We calculate the rates for momentum transfers $Q < 0.217/(A)^{\frac{1}{3}} \text{ GeV} \approx R_A^{-1}$ regime using the coherent EPA method. For intermediate momentum transfers $0.217/(A)^{\frac{1}{3}} \text{ GeV} \lesssim Q \lesssim M_p$ transfers, we use the diffractive EPA treatment. Finally for $Q \gtrsim 1 \text{ GeV} \approx M_p$ we

employ the deep inelastic formalism. We use PDFs from the MSTW collaboration (2008 NNLO best fit) [14]. To calculate the rates, we estimate the number of SM neutrino trident events for each flavour of incident neutrino ν_i producing a lepton pair composed of j^- and k^+ with $i, j, k \in \{e, \mu, \tau\}$. We estimate the luminosity in terms of charged current events N_{CC}^i using

$$N_{\text{Trident}}^{ijk} = \sum_E \frac{N_{CC}^i(E)}{\sigma_{CC}(E, A)} \sigma_{\nu A}^{ijk}(E, Z, A) \times \epsilon_-^j \times \epsilon_+^k, \quad (9)$$

where σ_{CC} is the neutrino charged current cross sections [17] and i, j, k are flavours denoting the incident neutrino, outgoing ℓ^- and outgoing ℓ^+ respectively. Additionally ϵ_+ and ϵ_- are the identification efficiencies for ℓ^+ and ℓ^- respectively. We do an analogous procedure for anti-neutrinos.

There will be a background contribution to trident from resonant production of charged pions and charm production from D mesons, whose leptonic modes are both dominated by muon flavoured final states. In the different flavour opposite sign di-lepton final states, backgrounds can arise from $\bar{\nu}_\mu$ CC scattering in combination with an elastic NC event releasing an electron, and also by muon final states in which one of the muons fake an electron. As coherent-scattering is quasi-elastic, the backgrounds for the dominant contribution to the cross section (see Section II B) can be greatly reduced by imposing hadronic vetoes in the analysis. Further background suppression can be achieved by selecting oppositely charged leptons that fall within the vertex resolution of the detectors and selecting events with low $M_{\ell^+\ell^-}$ invariant masses. We leave the background estimates to the collaborations' detailed and sophisticated simulations. Our signal results are shown in Tables II to IV.

A. Calibrations and Tests

The details of our calculations can be found in the Appendices. We calibrated our EPA cross section calculations with previous theoretical and experimental work [2, 10, 11], and reproduced the analytic results of [2].

Our DIS work was calibrated with MadGraph5 [3] for trident induced muon pair production. MadGraph5 treats light leptons as massless, and due to infrared singularities in the propagators this necessitates a careful treatment; it also introduces questions of reliability. We imposed the following cuts to replicate the effects of finite muon masses: $p_T > m_\mu$ for the muons, $p_T > 1.5$ GeV for the jets, and $\Delta R = \sqrt{\Delta\eta^2 + \Delta\phi^2} > 0.4$ for the lepton pairs. With these cuts we found our calculations to agree with MadGraph5 to within a factor of 0.5 – 2.5 for $E_\nu = \{20 \text{ GeV}, 200 \text{ GeV}, 1000 \text{ GeV}\}$. We believe our calculation to be more reliable than MadGraph5 in the low Q^2 regions of phase space which dominate the cross sections due to infrared divergences, which we treat carefully.

Neutrino Beam			Anti-Neutrino Beam		
Process	Coh	Diff	Process	Coh	Diff
$\nu_\mu \rightarrow \nu_e e^+ \mu^-$	85.46	24.6	$\bar{\nu}_\mu \rightarrow \bar{\nu}_e e^- \mu^+$	29.96	9.61
$\nu_\mu \rightarrow \nu_\mu e^+ e^-$	28.28	5.32	$\bar{\nu}_\mu \rightarrow \bar{\nu}_\mu e^+ e^-$	22.48	3.58
$\nu_e \rightarrow \nu_e e^+ e^-$	21.69	2.95	$\bar{\nu}_e \rightarrow \bar{\nu}_e e^+ e^-$	15.65	2.45
$\nu_e \rightarrow \nu_\mu \mu^+ e^-$	9.1	2.31	$\bar{\nu}_e \rightarrow \bar{\nu}_\mu \mu^- e^+$	14.31	3.16
$\nu_\mu \rightarrow \nu_\mu \mu^+ \mu^-$	4.79	3.01	$\bar{\nu}_\mu \rightarrow \bar{\nu}_\mu \mu^+ \mu^-$	3.76	2.38
$\nu_e \rightarrow \nu_e \mu^+ \mu^-$	0.42	0.16	$\bar{\nu}_e \rightarrow \bar{\nu}_e \mu^+ \mu^-$	0.3	0.12
$\nu_\tau \rightarrow \nu_\tau e^+ e^-$	0.13	0.03	$\bar{\nu}_\tau \rightarrow \bar{\nu}_\tau e^+ e^-$	0.13	0.02
$\nu_\tau \rightarrow \nu_\tau \mu^+ \mu^-$	0.01	0.	$\bar{\nu}_\tau \rightarrow \bar{\nu}_\tau \mu^+ \mu^-$	0.01	0.
$\nu_\tau \rightarrow \tau^- \mu^+ \nu_\mu$	0.	0.01	$\bar{\nu}_\tau \rightarrow \tau^+ \mu^- \bar{\nu}_\mu$	0.	0.
$\nu_\mu \rightarrow \mu^- \tau^+ \nu_\tau$	0.	0.23	$\bar{\nu}_\mu \rightarrow \mu^+ \tau^- \bar{\nu}_\tau$	0.	0.39
Total	149.88	38.62		86.6	21.71

TABLE II: Number of expected trident events for coherent (Coh) and diffractive (Diff) scattering, using the EPA, in the **SHiP** ν_τ detector, assuming 2×10^{20} POT on molybdenum.

B. Rates for SHiP

SHiP will be a lead based neutrino detector [5, 19]. It will utilize an emulsion cloud chamber for its electron detection and a muon magnetic spectrometer for muons. It is estimated to have a 90% e and μ identification efficiency, and a micron vertex resolution. Under nominal operating conditions, after 5 years of operation it will have collected data from 2×10^{20} POT using a 400 GeV SPS proton beam. We quote all the rates assuming this normalization.

The energy spectrum at SHiP is very broad, and reaches sufficiently high energies such that trident production of tau leptons becomes kinematically allowed in the coherent, diffractive, and deep inelastic regimes. The latter is allowed at almost all incident neutrino energies available at SHiP with the only requirement being the centre of mass energy exceed the lepton pair's mass-gap. Despite being kinematically allowed, we find the large momentum transfer in the deep inelastic regime renders the contribution to the cross section negligible. The diffractive and coherent regimes rely on the high energy tail of the quoted beam distribution [19]. For electrons and muons, coherent, and diffractive production are not only possible but extremely viable, while for tau leptons we find only diffractive production to be viable, but only marginally so. In Fig. 3 and Fig. 7, we show the cross section per nucleon as a function of the incoming neutrino energy for a variety of processes. The coherent cross sections computed via the EPA are normalized by Z^2 while the deep inelastic contribution is normalized by A . There are small differences in these plots for various materials, as the EPA Woods-Saxon form factor and

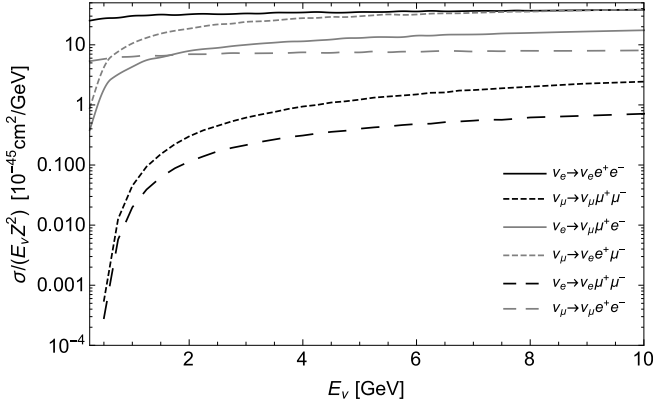


FIG. 4: σ/E_ν trident cross sections normalized by Z^2 for various SM flavours as a function of the incoming neutrino energy on an argon target (DUNE).

SM this is maximal in the case of W mediated interactions, intermediate for $W+Z$ mediated interactions, and minimal for Z mediated interactions. The W exclusive channel corresponds to scattering events where the incoming and outgoing neutrino belong to different lepton generations, and thus these channels will be more probable. Another dominant feature controlling the relative size of cross sections is related to the masses of the outgoing leptons. This dictates the size of the logarithmic enhancement coming from the low Q^2 phase space. This is a feature of the IR divergence arising from the photon propagator, which is regulated by the finite masses of the charged leptons. Finally the rates quoted in Tables II to IV are further influenced by beam luminosity, and so tend to favour incident muon configurations, except at the DUNE far detector, where they favour incident electron neutrinos.

These qualitative features suggest that $\nu_\mu \rightarrow \nu_e \mu^- e^+$ would serve as the dominant production mode at both the DUNE near detector and SHiP. Examining Tables II and III, this is indeed the case. It is a CC-exclusive process (high axial-vector couplings), it benefits from the large flux of muon neutrinos, and from the logarithmic enhancement afforded by the low electron mass. This final statement is most important at DUNE due, to its lower $\langle E_\nu \rangle$, which makes it sensitive to muon-mass threshold effects. For diffractive processes the sensitivity of the cross section to the charged lepton masses is weakened due to the lower bound Q_{\min} in Eq. (6). This accounts for the difference in ordering of rates between the coherent and diffractive contributions to the cross section found in Tables II to IV. At DUNE this results in an enhancement of the cross section by a factor of 35 when compared to the production mode $\nu_\mu \rightarrow \nu_\mu \mu^+ \mu^-$, which was observed at CHARM-II, CCFR, and NuTeV [10, 11, 16]. No dedicated search was carried out for electron production in trident modes at these experiments. The detector technology typically consisted of interwoven layers of heavy element materials to induce neutrino in-

teractions, followed by calorimeters to measure the final lepton states. Electrons create showers and scatter much more in these layers, as opposed to muons which tend to follow a straight trajectory until the muon spectrometer. It was thus much more difficult to impose vertex requirements on electrons, which is an integral part of the trident analysis. Neutrino detector technology has greatly evolved since then, and it is now feasible to consider mixed flavour trident channels.

The lifetime expected event count for $\mu^+ \tau^-$ and $\mu^- \tau^+$ production are both approximately unity. Given the uncertain run-time and technical specifications of SHiP it is possible that tridents containing tau leptons will occur, however the rates are sufficiently low that it is not clear at what level of statistical significance these can be observed, especially after applying necessary cuts. Our analysis suggest that these events are most likely to occur for intermediate momentum transfers (i.e. in the diffractive regime). Our deep inelastic analysis revealed high- Q^2 trident production to be extremely suppressed for all flavours, including tau leptons. ν_τ induced electron-muon pairs may be observable, however, due to the much higher flux of ν_μ 's this channel will be dominated by ν_μ induced events with identical charged lepton final states, which will leave an indistinguishable signature in the detector.

In the case of the DUNE collaboration, the size of the near detector is currently being planned such that it can obtain approximately ten times the statistics of the far detector; allowing for a reduction in the systematic uncertainties of the neutrino beam. Our results show that even for near detector masses that minimally satisfy this requirement trident production should be detectable. Given the large beam intensity at the near detector, every additional unit of detector mass represents a fantastic return on investment from the perspective of rare neutrino processes such as trident production. Pushing from hundreds to thousands of events would lower statistical error to the level of a few percent, and could potentially allow for trident production to act as a complimentary beam characterization tool. This is alluring because trident production is only sensitive to the target nucleus' electric form factor, in contrast to CC events where uncertainties in the axial form factor still introduce significant systematic effects.

While interesting in its own right as a test of the Standard Model, neutrino trident production can also act as a significant background in the search for new physics. This is because of its qualitative similarities to processes involving lepton flavour violation, which is a signature of many BSM models. Our estimated rates also suggest that both SHiP and the DUNE near detector can be used to constrain BSM physics; comparison with the number of events identified by the CCFR, and CHARM-II collaboration in the di-muon channel alone demonstrates that both SHiP and DUNE are competitive with these previous experiments. With access to flavour dependent final states, however, we believe these experiments can do much better. For example the Z' coupling to $L_\mu - L_\tau$

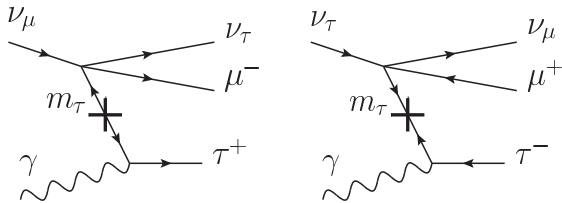


FIG. 5: Inequivalent contributions to the processes $\nu_\mu \rightarrow \nu_\tau \tau^+ \mu^-$ (left) and $\nu_\tau \rightarrow \nu_\mu \mu^+ \tau^-$ (right) in the limit of $m_\mu \rightarrow 0$. Note that the chiral structure of the weak interaction results in a triplet of left-handed leptons (LLL) for incident ν_μ and a right-handed lepton pair with a left-handed neutrino (LRR) for incident ν_τ .

The fermions are two component spinors of definite chirality. Diagrammatic conventions are from [7] with arrows denoting chirality.

considered in [2] influences both $\nu_\mu \rightarrow \nu_\mu \mu^+ \mu^-$ and $\nu_\mu \rightarrow \nu_\mu e^+ e^-$. Due to the minimal size of $|C_V|^2 + |C_A|^2$ for $e^+ e^-$ production (due to Z-exclusive mediation) this process will experience an even greater relative sensitivity to new physics, albeit in a first-generation lepton channel.

Although the qualitative features discussed earlier are sufficient to understand the most prominent aspects of our analysis, a closer examination of Figs. 3 and 4 reveals another feature, which is initially surprising. The rates for processes which seem to be related by an exchange of flavour indices have different cross sections. This effect is $\mathcal{O}(1)$ and independent of energy (see Fig. 3 $\nu_\mu \rightarrow \nu_\tau \tau^+ \mu^-$ vs $\nu_\tau \rightarrow \nu_\mu \mu^+ \tau^-$ for example). This would seem to suggest a violation of lepton universality, however a closer examination reveals that the chiral structure of the outgoing leptons is not equivalent, with the amplitudes for production into inequivalent configurations being proportional to the square of the heaviest lepton mass. Still this effect is surprising given that it is independent of energy, and naively one would expect that at sufficiently high centre of mass energies the effect would be suppressed by m_ℓ^2/S with S the Mandelstam variable for the neutrino-nucleus interaction. This is not the case for trident production because the cross section is dominated by the low- Q^2 region of phase space. To understand this we turn to the EPA, and more specifically Eq. (3). We see that the integral over s has an IR cutoff of $m_{ij}^2 = (m_{\ell^+} + m_{\ell^-})^2$, and so in this regime we find an $\mathcal{O}(m_{ij}^2/s) \sim \mathcal{O}(1)$ contribution to the cross section, which will be present even for arbitrarily high E_ν .

To understand why the chiral structure of the amplitude has a significant impact on the amplitude we must consider both the infrared divergence of the photon mediator, and the constraints imposed by conservation of angular momentum. Consider the centre of mass frame for the photon-neutrino pair. To saturate the lower bound of the integral over s in Eq. (3) we must produce the lepton-pair at rest, and have the neutrino red-shift to

an arbitrarily small energy $E'_\nu = \epsilon$; this also forces the lepton pair to carry equal and opposite momentum. It is, however, difficult to understand the implications of chirality in this frame, because in this frame the lepton pair is non-relativistic and we cannot freely interchange helicity and chirality.

To solve this problem we can appeal to Lorentz invariance and perform the same analysis in a boosted frame in which the lepton-pair is highly relativistic. To do this boost in the direction of infinitesimal momentum for the lepton pair. This boost will further red-shift the outgoing neutrino, but it will not change its direction. We would like to check if this configuration conserves angular momentum, and the answer to this question is dependent on the initial polarization of the incident photon (the neutrino's polarization is fixed because of its definite chirality), which in turn determines the initial angular momentum. The two possibilities are $S = 1/2$ and $S = 3/2$.

As shown in Fig. 5 the outgoing states for the two configurations have different chirality (LLL vs LRR). In the case of $S = 1/2$ this has no effect on the configuration discussions above, however in the case of $S = 3/2$, where the spin of the neutrino and photon are aligned, the LLL configuration is forbidden, while the LRR configuration is allowed. This is because in our boosted frame, where chirality is equivalent to helicity, in order to obtain $S = 3/2$ for the LLL configuration all three particles would have to travel in the same direction, which would violate conservation of momentum. Thus only the LRR, and not the LLL, configuration satisfies all the necessary conservation laws in the low- Q^2 region of phase space that dominates Eq. (3).

V. CONCLUSIONS & OUTLOOK

We have demonstrated that as of yet unobserved neutrino trident processes are within reach with the planned DUNE and SHiP experimental collaborations. The DUNE collaboration may be able to enhance production modes, some of which we currently estimate to only yield 1 – 10 events in the experiment's lifetime (e.g. $\nu_\mu \rightarrow \nu_\mu \mu^+ \mu^-$), by increasing the mass of the relatively small near detector. Even with the current proposed designs both collaborations are maximally sensitive to the mode $\nu_\mu \rightarrow \nu_e \mu^- e^+$ and $\bar{\nu}_\mu \rightarrow \bar{\nu}_e \mu^+ e^-$. We believe that backgrounds for these searches will be low, especially given the vertex resolution of both experiments [1, 19].

In addition to our direct application to the DUNE and SHiP collaboration we also present $\sigma(E_\nu)$ for the coherent scattering regime, allowing for future analyses with more precise luminosity estimates. We present a similar plot in Fig. 7 in case high momentum-transfer trident is of future interest. We have considered all possible combinations of lepton flavour final states, and have presented only processes with non-zero lifetime event counts. This work is complementary to that found in [13], where differential distributions with respect to the lepton pair's invariant

mass are plotted in the coherent regime. Additionally we have demonstrated a method for treating neutrino trident production on the parton level, which requires some slight modifications to the standard treatment. This revealed high- Q^2 trident production is untenable as one would naïvely expect.

Neutrino trident production is a proven tool in the testing of the SM and constraining BSM physics, and with improved detector designs it is important to harness the full capabilities of next generation neutrino experiments. Our analysis suggests that both SHiP and DUNE will be able to observe trident production. We believe with these experiments on the horizon the future is bright for studying trident production and other rare neutrino processes, and that the study of these processes should be incorporated into the physics programs of both experiments.

ACKNOWLEDGEMENTS

We are very grateful to Maxim Pospelov for suggesting mixed flavour trident production and its applicability to future intensity frontier experiments. Additionally we would like to thank him for his continued guidance throughout this research. We would also like to thank Itay Yavin for his help in the treatment of phase space. Finally we thank Chien-Yi Chen and Richard Hill for useful discussions. This research was supported in part by Perimeter Institute for Theoretical Physics. Research at Perimeter Institute is supported by the Government of Canada through the Department of Innovation, Science and Economic Development and by the Province of Ontario through the Ministry of Research and Innovation. This research was also supported by funds from the National Science and Engineering Research Council of Canada (NSERC), the Ontario Graduate Scholarship (OGS) program, and the Early Research Awards program of Ontario.

Appendix A: 3-Body Phase Space (EPA)

For the purposes of the EPA, the phase space integrals are performed over the 3-body phase space of the leptons. Ultimately this 3-body phase space is embedded in the full 4-body one, and so we will use the results of this section in the proceeding one. We denote the centre of mass energy for the photon-neutrino collision by s , additionally we define the quantities $P = p_+ + p_-$ and $\ell = P^2$. We begin by decomposing the 3-body phase space using the identity below.

$$d\Phi_3(p_+, p_-, k_2) = \frac{d\ell}{2\pi} \Phi_2(k_2, P) \Phi_2(p_+, p_-). \quad (\text{A1})$$

Each two-body phase space can be expressed as

$$d\Phi_2(q_1, q_2) = \bar{\beta}(q_1, q_2) \frac{d\Omega}{32\pi^2} \quad (\text{A2})$$

with the definition

$$\bar{\beta}(q_1, q_2) = \sqrt{1 - \frac{2(q_1^2 + q_2^2)}{(q_1 + q_2)^2} + \frac{(q_1^2 - q_2^2)^2}{(q_1 + q_2)^4}} \quad (\text{A3})$$

An important case is when $q_1^2 = 0$. In this scenario the factor simplifies to $\bar{\beta} = 1 - \frac{q_2^2}{(q_1 + q_2)^2}$. In our decomposition above $\bar{\beta}(k_2, P) = 1 - \ell/s$. First we choose to evaluate $d\Phi_2(P, k_2)$ in the centre of mass frame of the reaction. This allows us to parameterize the phase-space as written in Eq. (A2). We can perform the azimuthal integration by appealing to symmetry, and we are left only with $d\cos\theta_{CM}$. This can conveniently be expressed in terms of the Lorentz-invariant t defined via

$$t = 2q_\mu(k_1 - k_2)^\mu = \frac{1}{2}(s + \ell + (\ell - s)\cos\theta_{CM}). \quad (\text{A4})$$

This definition leads to the differential relationship $dt = \frac{1}{2}(\ell - s)d\cos\theta$. Thus we can simplify our 3-body phase space integral by applying the identity $\bar{\beta}(k_2, P)d\cos\theta = -\frac{2}{s}dt$. This leaves us with the second phase space integral. This is most easily evaluated in the frame where P_μ has vanishing three-momentum. In this frame there is no guarantee of azimuthal symmetry in the matrix element, and so we must integrate over both polar angles. We are left with the expression quoted in [2]

$$d\Phi_3(k_2, p_+, p_-) = \frac{1}{2} \frac{1}{(4\pi)^2} \frac{d\ell}{2\pi} \bar{\beta}(p_+, p_-) \frac{dt}{2s} \frac{d\Omega}{4\pi} \quad (\text{A5})$$

where we denote the angular integral over the muon-pair, performed in the frame where $P = (\sqrt{\ell}, 0, 0, 0)$ by $d\Omega$. The limits of integration for t are given by $\ell < t < s$. This gives the expression for the photon-neutrino cross section as

$$\sigma_{\gamma\nu} = \frac{1}{2s} \frac{1}{2} \frac{1}{(4\pi)^2} \int_{m_{jk}^2}^s \frac{d\ell}{2\pi} \bar{\beta}_\pm(\ell) \int_\ell^s \frac{dt}{2s} \int \frac{d\Omega}{4\pi} |\overline{\mathcal{M}}|_{\gamma\nu}^2 \quad (\text{A6})$$

where $m_{jk} = m_j + m_k$, and $|\overline{\mathcal{M}}|^2 = 1/2 \sum_{\text{pol}} |\mathcal{M}|^2$.

To obtain the full cross section this must be weighted against the probability for creating a photon in the Coulomb field of a nucleus, given in [2, 4]. This leads to

$$\sigma_{N\nu} = \frac{Z^2\alpha}{\pi} \int_{m_{jk}^2}^s \frac{ds}{s} \sigma_{\gamma\nu}(s) \int_{(s/2E_\nu)^2}^\infty \frac{dQ^2}{Q^2} F^2(Q^2) \quad (\text{A7})$$

where \sqrt{s} denotes the neutrino-nucleus centre of mass energy. In practice, the form factor of the nucleus $F(Q^2)$ cuts this integral off near $s_{\text{max}} \approx 2E_\nu \Lambda_{\text{QCD}}/A^{1/3}$. In our calculations for the coherent regime (Section IIB 1) we used the Woods-Saxon form factor

$$F_{\text{WS}}(Q^2) = \frac{1}{N} \mathcal{F} \left\{ \frac{V_0}{1 + \exp\left(\frac{r-r_0 A^{1/3}}{a}\right)} \right\} \quad (\text{A8})$$

with \mathcal{F} denoting the Fourier transform with respect to r , and N is a normalization factor given by the volume integral over the nuclear charge distribution[12]. The various parameters are set as $r_0 \approx 1.126$ fm, $a \approx 0.523$ fm, and $V_0 = (4\pi Ar_0^3/3)^{-1}$. Different choices of form factor modify the result on the 10% level.

For the diffractive regime we used the electric dipole fit for the proton's Dirac form factor found in [6, 9, 18]. Due to the quasi-elastic nature of the scattering the Pauli form factor's contribution is suppressed. The explicit expression is given by

$$F_{\text{dip}}(Q^2) = \frac{G_{\text{dip}}(Q^2) + \tau \xi G_{\text{dip}}(Q^2)}{1 + \tau} \quad (\text{A9})$$

where $\tau = Q^2/4M^2$ with $M = (m_p + m_n)/2$ and $\xi = (\mu_p - \mu_n)/\mu_N \approx 4.7$ the difference in magnetic moments between the proton and the neutron measured in units of the nuclear magneton. The dipole fit is given by

$$G_{\text{dip}}(Q^2) = \left(1 + \frac{Q^2}{0.71 \text{ GeV}^2}\right)^{-2}. \quad (\text{A10})$$

Appendix B: 4-Body Phase Space (DIS)

1. Parton-Neutrino Collision

We now consider the decomposition of the 4-body phase space. This will involve a reduction to the previously analyzed 3-body case, however there will be some difference thereafter because of the loss of azimuthal symmetry in $\Phi_2(P, k_2)$.

We begin by emphasizing a change in notation. The centre of mass energy for the parton-neutrino collision is

denoted S , we introduce the four-vector $R = k_2 + p_+ + p_-$ and its invariant mass $L = R^2$, and we maintain the previous definition of $P = p_- + p_+$. We can now decompose the 4-body phase space as shown schematically in Fig. 6 and more precisely below:

$$\begin{aligned} & d\Phi_4(p_+, p_-, h_2, k_2) \\ &= \frac{dL}{2\pi} d\Phi_2(R, h_2) d\Phi_3(p_+, p_-, k_2) \\ &= \frac{dL}{2\pi} \frac{dL}{2\pi} d\Phi_2(R, h_2) \Phi_2(k_2, P) \Phi_2(p_+, p_-). \end{aligned} \quad (\text{B1})$$

The first two-body phase space $\Phi_2(h_2, R)$ inherits the azimuthal symmetry of the parton-neutrino collision, and in direct analogy with Eq. (A4) we introduce the variable T defined via

$$T = 2h_1^\mu (k_1 - h_2)_\mu = \frac{1}{2} [S + L + (L - S) \cos \theta_h]. \quad (\text{B2})$$

The final pair of two-body phase spaces do not inherit the azimuthal symmetry, and so we do not attempt to further simplify them. We therefore evaluate $d\Phi_2(k_2, P)$ and $d\Phi_2(p_+, p_-)$ in their respective rest frames. The angles of the charged lepton frame are labelled θ and ϕ while those of $\Phi_2(k_2, P)$ are labelled θ' and ϕ' . With these variables the four-body phase space can be written

$$d\Phi_4 = \frac{dL}{2\pi} \frac{4\pi}{32\pi^2} \frac{dT}{S} \frac{d\ell}{2\pi} \bar{\beta}(k_2, P) \bar{\beta}(p_+, p_-) \frac{d\Omega'}{32\pi^2} \frac{d\Omega}{32\pi^2}. \quad (\text{B3})$$

Keeping in mind that the Lorentz invariant flux factor \mathcal{F} for massless initial states is given by $\mathcal{F} = 2S$ we can express the parton cross section as

$$\sigma_{h\nu}(S) = \frac{1}{2S} \int_{m_{jk}^2}^S \frac{dL}{2\pi} \int_L^S \frac{2\pi}{32\pi^2} \frac{2}{S} \frac{dT}{S} \int_{m_{jk}^2}^L \frac{d\ell}{2\pi} \bar{\beta}(k_2, P) \bar{\beta}(p_+, p_-) \int \frac{d\Omega'}{32\pi^2} \int \frac{d\Omega}{32\pi^2} |\overline{\mathcal{M}}|_{h\nu}^2. \quad (\text{B4})$$

2. Hadron Neutrino Cross Section

We now connect our partonic cross section to the hadronic cross section via the formalism of deep inelastic scattering. We introduce the new variable S_H defined by $\xi S_H = S$ and is given by $S_H = 2E_\nu M_N$ in the lab frame. Unlike in textbook treatments of deep inelastic scattering, we cannot integrate ξ over the full interval $[0, 1]$ because we require a minimum amount of energy to produce the pair of charged leptons (i.e. $\xi \approx 0$ is kinematically forbidden). Additionally we would like to ensure that we do not double count amplitudes already included in the EPA and so we include a cut on the minimum amount of four-momenta transfer to the nucleus $Q > Q_{\text{min}}$.

To impose this cut it is easiest to change from the variable T to the variable $U = Q^2 = |q^2|$. If we place a cut on the momentum transfer $U > Q_{\text{min}}^2$ then this changes the bounds of integration in Eq. (B4). We chose $Q_{\text{min}} = 1\text{GeV}$ to ensure we are not double-counting amplitudes. However with this scheme we include a parametric regime in which hadronic resonances can be very important. Although the description in terms of partons may capture some of the essential features of hadron production it is probable that the DIS formalism underestimates the rates, because it does not incorporate resonance conditions.

The effects of a cut on momentum transfer can be seen by noting that $U = S - T$, and that the bounds of integration require $S > T > L$. The smallest L , and by proxy T ,

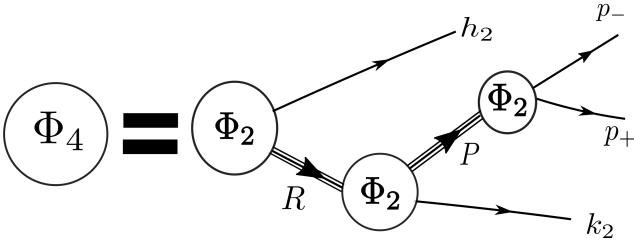


FIG. 6: Schematic depiction of the four-body phase space decomposition into three two-body phase spaces. Note the three-body phase space decomposition for the EPA is obtained by considering only the final two phase spaces in the diagram.

$$\sigma_{H\nu} = \sum_h \int_{\xi_{\min}}^1 \frac{d\xi}{2\xi S_H} \int_{m_{jk}^2}^{L_{\max}} \frac{dL}{2\pi} \int_{Q_{\min}^2}^{\xi S_H - L} \frac{1}{8\pi} \frac{dU}{\xi S_H} \int_{m_{jk}^2}^L \frac{d\ell}{2\pi} \int \frac{d\Omega}{32\pi^2} \frac{d\Omega'}{32\pi^2} |\overline{\mathcal{M}}|_{h\nu}^2 \overline{\beta}(k_2, P) \overline{\beta}(p_+, p_-) f_h^{(H)}(\xi, U) \quad (B6)$$

where h runs over all the partons in the given nucleon $H \in \{n, p\}$ (either neutrons or protons), $L_{\max} = \xi S_H - Q_{\min}^2$, ξ_{\min} saturates the bound in Eq. (B5) and $f_h^{(H)}(\xi, Q)$ is the parton distribution function for the parton h in H . To obtain the neutrino-nucleus cross section a simple weighted sum of individual nucleon cross sections was used

$$\sigma_{A\nu} = Z\sigma_{p\nu} + (A - Z)\sigma_{n\nu}. \quad (B7)$$

Appendix C: Luminosity Estimates

1. SHiP

For the purposes of calculating expected rates at SHiP we relied on Ref. [19]; specifically Figure 5.25 and Table 2.3. These quote the number of expected charged current events in the detector. To convert this into a neutrino luminosity we simply divided by the charged current cross section which we took to be given by

$$\sigma_{CC} = A \left(\frac{E_\nu}{\text{GeV}} \right) \begin{cases} 6.75 \cdot 10^{-39} \text{ cm}^2 & (\nu) \\ 3.38 \cdot 10^{-39} \text{ cm}^2 & (\overline{\nu}) \end{cases} \quad (C1)$$

with the braced numbers referring to incident neutrinos and anti-neutrinos respectively. To determine the experiment's lifetime integrated luminosity, we used the number of CC events from Table 2.3 of [19], while the energy spectrum was taken from Figure 5.25. Finally we multiplied by the detector's efficiency (which we took to be 90% for each of the final state leptons), leading to Eq. (9).

can be is m_{jk}^2 , which implies that $U = S - T < S - m_{jk}^2$. Combining this with the condition that $U > Q_{\min}$ leads to $S - m_{jk}^2 > Q_{\min}^2$. Finally this can be converted into a minimum bound on ξ given by

$$\xi \geq \frac{Q_{\min}^2 + m_{jk}^2}{S_H}. \quad (B5)$$

Finally we note that depending on the magnitude and direction of the individual leptons Q^2 could range from being very small, to $S - m_{jk}^2$ and so we must include the parton distribution functions inside the integral over U . This leads to our final expression for the nucleon-neutrino cross section

2. DUNE

The DUNE collaboration's far and near detectors are treated separately in their proposals, with a heavier emphasis on the far detector. As a result there is no published neutrino spectrum for the near detector, however both detectors have lifetime expected event counts. We therefore had to infer the near detector spectrum from that of the far detector, and then normalize our results to reproduce the lifetime rates quoted in Table 6.1 of [1].

To link the beam luminosity in the far detector to those in the near detector we also adjusted the various flavours' luminosity to account for oscillation effects. All ν_e appearances at the far detector were assumed to stem from ν_μ at the near detector, while $\nu_e + \overline{\nu}_e$ background in the far detector was assumed to represent the full flux of first generation neutrinos at the near detector up to geometric losses due to beam spread.

Additionally the CC rates in the DUNE proposal at the near detector are quoted per 10^{20} protons on target (POT) and one tonne of detector mass. The far detector rates are quoted assuming 150 kt-MW-yr. This number assumes a 40 kt far detector, and that 1.2 MW of beam power corresponds to 1.1×10^{21} POT/yr. We therefore multiply the event counts in Table 6.1 in [1] by

$$\frac{1.1 \times 10^{21} \text{ POT/yr}}{1.2 \text{ MW}} \times 850 \text{ kt-MW-yr} \times \frac{0.1 \text{ tonnes}}{40 \text{ kt}} \quad (C2)$$

where 850 kt-MW-yr is the exposure at the far detector in the lifetime of DUNE given the optimized design and 0.1 tonnes is the mass of the near detector.

Next we consider the details of the far detector. For this we use Figures 3.5, 3.29 and Table 3.5. Table 3.5 and Figure 3.5 are in correspondence with one another, and quote their results for an exposure of 150 kt-MW-yr. They specify different rates for the running of the exper-

iment in neutrino and anti-neutrino mode; we presume each mode constitutes half of the experiment's lifetime. We therefore adjust the rates quoted in Table 3.5 and Figure 3.5 of [1] by a factor of

$$\frac{850 \text{ kt-MW-yr}}{150 \text{ kt-MW-yr}} \times \frac{1}{2} \quad (\text{C3})$$

to obtain the lifetime event rate for the far detector. The spectrum is given in Figure 3.29 and here is quoted in units of CC-Events/GeV/kT/yr. The experiment is set to obtain an exposure of 300 kt-MW-yr at 1.07 MW and then 550 kt-MW-yr at 2.14 MW. Additionally the energy bin-width of the plot is 0.25 GeV and so we multiply the spectrum of Figure 3.29 of [1] by a factor of

$$\frac{0.25 \text{ GeV}}{1 \text{ bin}} \left(\frac{300 \text{ kt-MW-yr}}{1.07 \text{ MW}} + \frac{550 \text{ kt-MW-yr}}{2.14 \text{ MW}} \right). \quad (\text{C4})$$

Finally in Figure 3.29 the individual CC-event rates of ν_e and $\bar{\nu}_e$ are not given, but their sum is given. We assumed the relative ratio of neutrinos to anti-neutrinos was equal to the appearance rates quoted in Table 3.5 of [1]. Although the background neutrino rates are much smaller than the oscillation signal, they provide the dominant contribution at the near detector. The production fractions of K^+ and K^- kaons, denoted R_{K^\pm} have to be compared with those of π^+ and π^- , given as R_{π^\pm} .

We therefore assume that at the far detector the relative components of the $\nu_e + \bar{\nu}_e$ background are given by

$$N_{\nu_e}^{(\text{bkg})} = \frac{R_{\pi^+}}{R_{K^+}} \frac{N_{\nu_e}^{(\text{osc})}}{N_{\text{tot}}^{(\text{osc})}} N_{\text{tot}}^{(\text{bkg})} \quad (\text{C5a})$$

$$N_{\bar{\nu}_e}^{(\text{bkg})} = \frac{R_{\pi^-}}{R_{K^-}} \frac{N_{\bar{\nu}_e}^{(\text{osc})}}{N_{\text{tot}}^{(\text{osc})}} N_{\text{tot}}^{(\text{bkg})}. \quad (\text{C5b})$$

We then assume the first-generation component at the near detector is the progenitor of the full background signal at the far detector. Equivalently we estimate the number of electron and anti-electron events at the near detector to be proportional to N_{Bkg} at the far detector with an overall normalization that is consistent with geometric losses. To find the geometric loss factor we compared the rates for ν_μ CC events quoted in Table 6.1 of

[1] with the CC events from the ν_μ background signal and ν_e appearance signal quoted in Table 3.5 and Figure 3.5 of [1]. Our beam spectrum at the far detector was taken from Figures 3.29 and 3.5 of [1].

Appendix D: Deep Inelastic Scattering Results

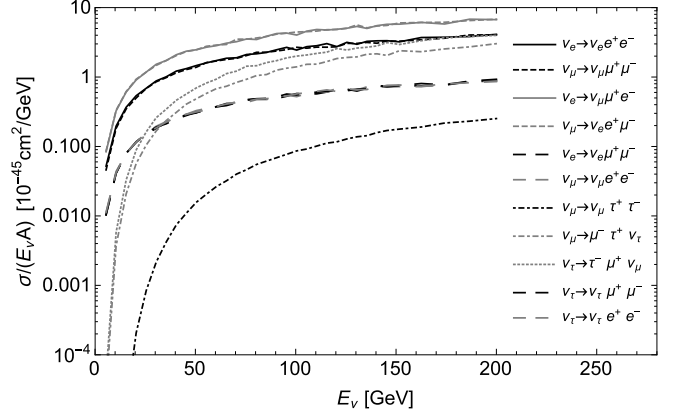


FIG. 7: σ/E_ν trident DIS cross sections per nucleon for various SM flavours as a function of the incoming neutrino energy on a lead target (SHiP).

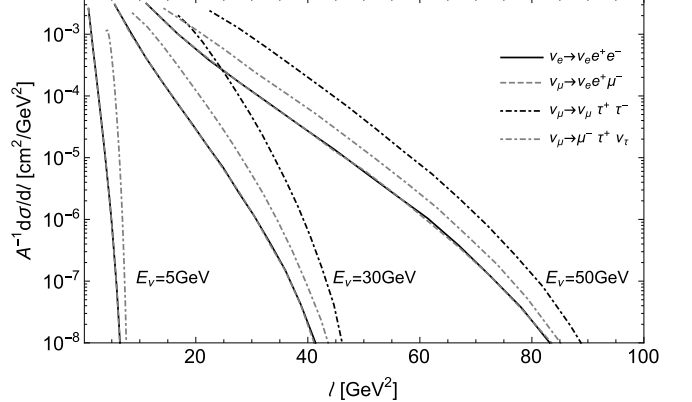


FIG. 8: Normalized $d\sigma/dl$ for a variety of DIS processes at SHiP, where $l = (p_{l^+} + p_{l^-})^2$. Energies are in GeV.

- [1] R. Acciarri and *et. al.* Long-Baseline Neutrino Facility (LBNF) and Deep Underground Neutrino Experiment (DUNE) Conceptual Design Report Volume 2: The Physics Program for DUNE at LBNF. 2, 2015.
- [2] W. Altmannshofer, S. Gori, M. Pospelov, and I. Yavin. Neutrino Trident Production: A Powerful Probe of New Physics with Neutrino Beams. *Phys.Rev.Lett.*, 113:91801, 2014.

- [3] J. Alwall, R. Frederix, S. Frixione, V. Hirschi, F. Maltoni, O. Mattelaer, H. S. Shao, T. Stelzer, P. Torrielli, and M. Zaro. The automated computation of tree-level and next-to-leading order differential cross sections, and their matching to parton shower simulations. *J. High Energy Phys.*, 2014(7), 2014.
- [4] R. Belusevic and J. Smith. W-Z interference in ν -nucleus scattering. *Physical Review D*, 37(9):2419–2422, 1988.

- [5] W. Bonivento, a. Boyarsky, H. Dijkstra, U. Egede, M. Ferro-Luzzi, B. Goddard, a. Golutvin, D. Gorbunov, R. Jacobsson, J. Panman, M. Patel, O. Ruchayskiy, T. Ruf, N. Serra, M. Shaposhnikov, and D. Treille. Proposal to Search for Heavy Neutral Leptons at the SPS. pages 1–21, 2013.
- [6] R. W. Brown, R. H. Hobbs, J. Smith, and N. Stanko. Intermediate boson. III. Virtual-boson effects in neutrino trident production. *Phys. Rev. D*, 6(11):3273–3292, 1972.
- [7] H. K. Dreiner, H. E. Haber, and S. P. Martin. Two-component spinor techniques and Feynman rules for quantum field theory and supersymmetry. *Phys.Rept.*, 494:1–196, 2010.
- [8] A. Drukier and L. Stodolsky. Principles and applications of a neutral-current detector for neutrino physics and astronomy. *Phys. Rev. D*, 30(11):2295–2309, 1984.
- [9] J. A. Formaggio and G. P. Zeller. From eV to EeV: Neutrino cross sections across energy scales. *Reviews of Modern Physics*, 84(3):1307–1341, 2012.
- [10] D. Geiregat, P. Vilain, G. Wilquet, U. Binder, H. Burkard, W. Flegel, H. Grote, T. Mouthuy, H. Øverås, J. Panman, A. Rozanov, K. Winter, G. Zacek, V. Zacek, R. Beyer, F. W. Büsser, C. Foos, L. Gerland, T. Layda, F. Niebergall, G. Rädcl, P. Stähelin, A. Tadsen, T. Voss, D. Favart, G. Grégoire, E. Knoop, V. Lemaître, P. Gorbunov, E. Grigoriev, V. Khovansky, A. Maslennikov, W. Lippich, A. Nathaniel, H. Neumeyer, A. Staude, J. Vogt, M. Caria, C. Cicalò, B. Eckart, A. G. Cocco, A. Ereditato, G. Fiorillo, S. Mennella, V. Palladino, P. Paolucci, P. Strolin, A. Capone, D. De Pedis, E. Di Capua, U. Dore, A. Frenkel-Rambaldi, P. F. Loverre, D. Macina, G. Piredda, R. Santacesaria, and D. Zanello. Calibration and performance of the CHARM-II detector. *Nucl. Inst. Methods Phys. Res. A*, 325(1-2):92–108, 1993.
- [11] D. Geiregat, G. Wilquet, U. Binder, H. Burkard, U. Dore, W. Flegel, H. Grote, T. Mouthuy, H. Overas, J. Panman, R. Santacesaria, P. Vilain, K. Winter, G. Zacek, V. Zacek, and R. Beyer. First Observation of Neutrino Trident Production. Technical report, CERN, 1990.
- [12] U. D. Jentschura and V. G. Serbo. Nuclear form factor, validity of the equivalent photon approximation and Coulomb corrections to muon pair production in photon-nucleus and nucleus-nucleus collisions. *Eur. Phys. J.*, C64:309–317, 2009.
- [13] J. Løvseth and M. Radomski. Kinematical distributions of neutrino-produced lepton triplets. *Physical Review D*, 3(11):2686–2706, 1971.
- [14] A. D. Martin, W. J. Stirling, R. S. Thorne, and G. Watt. Parton distributions for the LHC. *Eur. Phys. J.*, C63:189–285, 2009.
- [15] S. R. Mishra, S. A. Rabinowitz, C. Arroyo, K. T. Bachmann, R. E. Blair, C. Foudas, B. J. King, W. C. Lefmann, W. C. Leung, E. Oltman, P. Z. Quintas, F. J. Sciulli, B. G. Seligman, M. H. Shaevitz, F. S. Merritt, M. J. Oreglia, B. A. Schumm, R. H. Bernstein, F. Borcherdling, H. E. Fisk, M. J. Lamm, W. Marsh, K. W. B. Merritt, H. Schellman, D. D. Yovanovitch, A. Bodek, H. S. Budd, P. De Barbaro, W. K. Sakumoto, P. H. Sandler, and W. H. Smith. Neutrino tridents and W-Z interference. *Physical Review Letters*, 66(24):3117–3120, 1991.
- [16] NuTeV Collaboration and T. Adams. Neutrino Trident Production from NuTeV. page 4, 1998.
- [17] K. A. Olive et al. Review of Particle Physics. *Chin. Phys.*, C38:090001, 2014.
- [18] C. F. Perdrisat, V. Punjabi, and M. Vanderhaeghen. Nucleon Electromagnetic Form Factors. *Prog.Part.Nucl.Phys.*, 59:694–764, 2006.
- [19] SHiP Collaboration. A facility to Search for Hidden Particles (SHiP) at the CERN SPS. (April), 2015.
- [20] M. I. Vysotsky, I. V. Gaidaenko, and V. A. Novikov. On Lepton-Pair Production in Neutrino-Nucleus Collisions. 65(9):1676–1684, 2002.
- [21] I. Yavin. Private communication.